



Flexible belt hanging on two pulleys: Contact problem at non-material kinematic description

Yury Vetyukov^{a,*}, Evgenii Oborin^b, Jakob Scheidl^a, Michael Krommer^a,
Christian Schmidrathner^a

^aInstitute of Mechanics and Mechatronics, Vienna University of Technology, Getreidemarkt 9, Vienna A-1060, Austria

^bInstitute of Technical Mechanics, Johannes Kepler University, Altenbergerstraße 69, Linz A-4040, Austria

ARTICLE INFO

Article history:

Received 17 October 2018

Revised 26 March 2019

Available online 29 March 2019

Keywords:

Belt drive mechanics

Mixed Eulerian–Lagrangian description

Finite element analysis

Contact problem

Kirchhoff rod theory

ABSTRACT

We propose a non-material finite element scheme for modelling large deformations of a closed flexible rod supported by two rigid pulleys in the field of gravity. The mixed Eulerian–Lagrangian kinematic description of circumferential and transverse displacements is beneficial for simulations of moving belt drives. The necessary C^1 inter-element continuity in a compound coordinate system with Cartesian and polar domains requires a nonlinear finite element approximation. The theoretically predicted singular reaction force distribution prevents us from using the technique of Lagrange multipliers for normal contact. A novel semi-analytical solution of the static problem based on the integration of the equations of the nonlinear theory of rods in the free spans as well as in the segments of contact with pulleys is presented for the sake of validation. We demonstrate the mutual convergence of simulation results for a benchmark problem and additionally justify them by comparison against conventional Lagrangian finite element solutions.

© 2019 Elsevier Ltd. All rights reserved.

1. Introduction

We consider a symmetric, planar belt drive with two equal pulleys. Modelling the deflection of the belt in the field of gravity becomes challenging when the system starts moving. Referring the interested reader to a detailed discussion of the voluminous literature on axially moving continua and Eulerian (spatial) kinematic description in structural mechanics to Chen (2005), Vetyukov et al. (2016), Vetyukov et al. (2017a) and Vetyukov (2018), here we point out the intrinsic drawbacks of conventional finite element schemes with Lagrangian (material) kinematics when applied to the considered sort of problems as for example done by Dufva et al. (2007). Letting the finite element mesh move between the qualitatively different domains, namely the free spans and the zones of sticking or sliding contact between the belt and the pulleys, one inevitably experiences numerically induced oscillations in the solution, see also the benchmark example in Oborin et al. (2018). Moreover, material description implies regular re-meshing if a finer discretization is desired near the contact domains of a long belt drive, thus impacting the efficiency and accuracy of the analysis.

For a simpler model with only contour motion of the belt, the advantages of the Eulerian kinematic description have been demonstrated in Eliseev and Vetyukov (2012) and Vetyukov et al. (2017b) for transient dynamics with idealized friction, in Rubin (2000), Bechtel et al. (2000) and Morimoto and Iizuka (2012) for stationary (steady state) dynamics with exact resolution of the friction law and in Oborin et al. (2018) for a transient quasi-static analysis with time variation of the zones of stick and slip. For multi-dimensional deformations of axially moving structures, axial and transverse deflections may be efficiently separated using mixed Eulerian–Lagrangian kinematic description. The corresponding non-material finite element scheme follows with a change of variables in the variational equation of the principle of virtual work, see Steinbrecher et al. (2017) and Vetyukov (2018) for large vibrations of axially moving strings and beams as well as (Vetyukov et al., 2016) for transient quasistatic analysis of buckling and supercritical deformations of axially moving plates. A simple option for the change of variables is that one of the material coordinates (actually, the only one in the case of a string/beam) is considered as a nodal unknown and the spatial coordinate, along which the axial motion takes place, is fixed. The finite element mesh resides in a space with both spatial and material coordinates, and is thus always conforming to the boundary conditions. As an alternative, we also mention the idea of using a redundant set of nodal unknowns featuring spatial and material coordinates and

* Corresponding author.

E-mail address: yury.vetyukov@tuwien.ac.at (Y. Vetyukov).

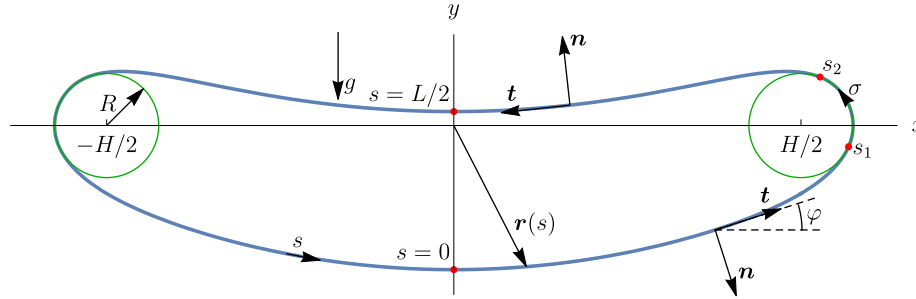


Fig. 1. Belt hanging on two pulleys: geometry and characteristic points.

using problem specific constraints with corresponding Lagrange multipliers, see [Hong and Ren \(2011\)](#) and [Liu et al. \(2019\)](#) online first, ([Escalona et al., 2018](#)). For an example of change of variable directly in the differential equations of rod mechanics in the context of the contact problem of motion of a rod within a curved channel we refer to [Denoël and Detournay \(2011\)](#), see also ([Huynen et al., 2016](#)) for an extension to the three-dimensional case with a helical tube.

In the present paper, we apply the mixed Eulerian–Lagrangian kinematic description for the first time to a closed rod with the help of a particular problem-specific coordinate system, composed of domains with Cartesian and polar coordinates. Introduced to separate the circumferential motion from transverse deflections, this combined parametrization of space is, however, only C^0 continuous, which is insufficient for the kinematics of Kirchhoff rods. We achieve the necessary smoothness between the elements by using a nonlinear finite element approximation. While the benchmark problem considered below is yet static and restricted to frictionless contact between the belt and the pulleys, the newly developed framework allows for a straightforward extension to transient simulations with rotating pulleys, friction and moving belt. More sophisticated practically relevant simulation scenarios as e.g. three-dimensional analysis with a shell model of the belt and various kinds of imperfections will also rest upon the present formulation.

We begin the narration with a novel semi-analytical solution, that extends the previously published analysis of a contact problem with no gravity ([Belyaev et al., 2017a](#)), and further

- demonstrates the use of the nonlinear equations of Kirchhoff rods for a contact problem,
- clearly shows the appearance of concentrated contact interactions (which has previously been reported by [Denoël \(2008\)](#), and which is not the case for shear-deformable rods, see [Belyaev et al. \(2018\)](#)),
- provides a solid theoretical background as well as reference values for validating the finite-element results.

A short version of the actual contribution has been presented at 89th Annual Meeting of GAMM and briefly published in [Scheidl et al. \(2018\)](#).

2. Statement of the problem and basic equations

A belt mounted on two pulleys is modelled as a closed, extensible rod with undeformed length L , bending stiffness a and extensional stiffness b . The belt has no own curvature and is straight when undeformed, see [Belyaev et al. \(2017a,b; 2018\)](#) for a circular undeformed state. Hanging in the field of gravity, the belt is supported by two horizontally arranged pulleys with the radius R and center distance H , see [Fig. 1](#). The present consideration is restricted to a static problem with a frictionless normal contact. Considering the belt as a material line, we parametrize it by the position vector

of particles

$$\mathbf{r}(s) = x(s)\mathbf{i} + y(s)\mathbf{j}. \quad (1)$$

This is a function of the material coordinate s , which is the length coordinate in the undeformed state and is counted counter-clockwise from 0 to L ; \mathbf{i} and \mathbf{j} are the unit basis vectors of the Cartesian coordinates x, y . We choose $s = 0$ in the bottom point of the lower free span, which coincides with the material point $s = L$ of the endless belt. The material point $s = L/2$ will always remain in the middle of the upper free span because of symmetry. The touching points s_1 and s_2 mark the borders of the region, in which the belt comes into contact with the surface of the right pulley. Certainly, existence of a line contact between a rod and a rigid obstacle cannot be postulated *a priori* and needs to be proven as a part of the solution, see discussions and experimental validation in [Goss and Chaouki \(2016\)](#), [Batista \(2017\)](#) and [Chen and Hua \(2018\)](#). Because of the bending stiffness, the configuration of the hanging belt in the free spans between the pulleys is different from the known catenary curves, which is most pronounced near the touching points.

The subsequent analysis relies on a geometrically nonlinear theory of rods, which follows from the principle of virtual work for extensible but unshearable plane material lines ([Antman, 1972; Eliseev, 2006; Vetyukov, 2012](#)). Three groups of equations are involved: balance (equilibrium), kinematic expressions for the strain measures and constitutive relations.

Adjacent particles of the belt interact through the force \mathbf{Q} and the bending moment M , which obey the balance equations

$$\begin{aligned} \mathbf{Q}' + \mathbf{q} &= 0, \\ M' + \mathbf{k} \cdot \mathbf{r}' \times \mathbf{Q} + m &= 0. \end{aligned} \quad (2)$$

The external forces \mathbf{q} and moments m are counted per unit material length s , $\mathbf{k} = \mathbf{i} \times \mathbf{j}$ is the unit out-of-plane vector and prime $(\cdots)'$ means a derivative with respect to s . With each particle of the rod we associate the unit tangent vector \mathbf{t} and the unit normal vector $\mathbf{n} = \mathbf{t} \times \mathbf{k}$. Projections

$$Q_1 = \mathbf{Q} \cdot \mathbf{t}, \quad Q_2 = \mathbf{Q} \cdot \mathbf{n} \quad (3)$$

are the axial tension force and the transverse shear force in the belt. The external forces

$$\mathbf{q} = -\rho g \mathbf{j} + p \mathbf{n} \quad (4)$$

are constituted by the gravity (ρ is the density per unit length and g is the free fall acceleration) and by the contact pressure p in the contact domain. Due to the absence of friction we assume $m = 0$ everywhere.

In the present paper we use the Green–Lagrange measure for the tensile strain

$$\varepsilon = \frac{1}{2} (\mathbf{r}' \cdot \mathbf{r}' - 1), \quad (5)$$

which determines the stretch D of the belt's axis:

$$\mathbf{r}' = D \mathbf{t}, \quad D \equiv \sqrt{1 + 2\varepsilon}. \quad (6)$$

A frequently used alternative is the Biot strain measure

$$\varepsilon_{\text{Biot}} = |\mathbf{r}'| - 1, \quad D = 1 + \varepsilon_{\text{Biot}}, \quad (7)$$

see [Eliseev and Vetyukov \(2012\)](#) for a detailed discussion of advantages and disadvantages of both. The Green–Lagrangian one is preferred, because it is easier to use in a finite element framework.

The bending strain measure is the material curvature

$$\kappa = -\mathbf{n} \cdot \mathbf{r}''/D = \varphi', \quad (8)$$

where within the classical theory of unshearable rods φ denotes the angle of rotation of a particle coinciding with the angle between the tangent vector \mathbf{t} and the horizontal axis x , see [Fig. 1](#). The geometric curvature of the line $\mathbf{r}(s)$ differs from κ by the factor D because of extension.

Finally, we arrive at the constitutive law featuring the strain energy per unit material length approximated by a quadratic form

$$U = \frac{1}{2}a\kappa^2 + \frac{1}{2}b\varepsilon^2. \quad (9)$$

The component Q_1 is a work-conjugate for $\varepsilon_{\text{Biot}}$ and not for ε , hence, the constitutive relations read

$$Q_1/D \equiv \hat{Q}_1 = b\varepsilon, \quad M = a\kappa. \quad (10)$$

Clearly, one could introduce U as a quadratic form of $\varepsilon_{\text{Biot}}$, which would slightly simplify the above formulas, but otherwise not affect the finite element analysis. For a comparison of the two variants and a thorough discussion of the difference between Q_1 and \hat{Q}_1 we again refer to [Eliseev and Vetyukov \(2012\)](#). A constitutive relation for the shear force Q_2 cannot be written and is not necessary.

3. Semi-analytic solution

In this section we will formulate a boundary value problem (BVP) for the contact problem of hanging the belt on the pulleys and solve it numerically. Equations from [Section 2](#) are conveniently summarized in the form

$$\hat{Q}_1' D + \frac{\hat{Q}_1 \hat{Q}_1'}{bD} + \varphi' Q_2 - \rho g \sin \varphi = 0,$$

$$Q_2' - \varphi' \hat{Q}_1 D + \rho g \cos \varphi + p = 0,$$

$$M' - D Q_2 = 0, \quad (11)$$

$$\mathbf{r}' = D(\mathbf{i} \cos \varphi + \mathbf{j} \sin \varphi), \quad \varphi' = a^{-1} M, \quad (12)$$

$$D = \sqrt{1 + 2b^{-1} \hat{Q}_1}, \quad \hat{Q}_1 = D^{-1} \mathbf{Q} \cdot \mathbf{t}, \quad (13)$$

where we have used the component representation of \mathbf{Q} to project the first equilibrium equation onto \mathbf{t} and \mathbf{n} as well as to simplify the balance of moments. The external forces are replaced with [Eq. \(4\)](#).

We divide the considered right half of the belt into three segments: two free spans (lower one with $0 \leq s \leq s_1$ and upper one with $s_2 \leq s \leq L/2$) and the contact segment $s_1 \leq s \leq s_2$ in between, see [Fig. 1](#). In the following, we will treat the above system for each of these segments separately. In order to achieve a BVP with fixed boundaries we will introduce a new dimensionless coordinate. Finally, the matching conditions between the segments and the symmetry considerations will provide sufficient boundary conditions to completely state the problem.

3.1. Contact segment

At the beginning we introduce a spatial (arc) coordinate σ , counted from the rightmost point of the pulley with $x = H/2 + R$, $y = 0$. It is defined as function of the material coordinate s in the contact segment $s_1 \leq s \leq s_2$ according to the following relations:

$$\mathbf{r}'(s) ds = \partial_\sigma \mathbf{R}(\sigma) d\sigma, \quad |\partial_\sigma \mathbf{R}| = 1,$$

$$\sigma' = |\mathbf{r}'| = D, \quad \partial_\sigma s = D^{-1} \quad (14)$$

with $\mathbf{R}(\sigma)$ being the parametrization of the circular line of contact (surface of the right pulley):

$$\mathbf{R} = (H/2 + R \cos(\sigma/R))\mathbf{i} + R \sin(\sigma/R)\mathbf{j}. \quad (15)$$

We assume full contact, meaning that every particle of the considered belt segment lies on the pulley circle.

Since there is no shear, the rotation angle φ is a known function of the arc coordinate σ :

$$\varphi = \pi/2 + \sigma/R,$$

$$\varphi' = \sigma'/R = D/R. \quad (16)$$

From the elasticity relation [Eq. \(12\)](#) we obtain the moment and then use [Eq. \(13\)](#) to find its derivative:

$$M = \frac{aD}{R},$$

$$M' = \frac{a\hat{Q}_1'}{bRD}. \quad (17)$$

Comparing the balance of moments [Eqs. \(11\)–\(17\)](#), we find the transverse force Q_2 :

$$Q_2 = \frac{a\hat{Q}_1'}{bRD^2}. \quad (18)$$

We now substitute Q_2 from [Eq. \(18\)](#) and φ' from [Eq. \(16\)](#) into the first balance equation [Eq. \(11\)](#) and arrive at the differential equation for \hat{Q}_1 as follows:

$$\hat{Q}_1' = \rho g b R^2 \sin \varphi \frac{D}{3R^2 \hat{Q}_1 + R^2 b + a}. \quad (19)$$

The second formula [Eq. \(11\)](#) gives the contact pressure

$$p = -Q_2' + R^{-1}(1 + 2b^{-1}\hat{Q}_1)\hat{Q}_1 - \rho g \cos \varphi, \quad (20)$$

which is to be determined after solving the equations. The pressure p needs to be non-negative in the present non-adhesive formulation, which is a prerequisite for the assumption of continuous line contact made above.

As a result, just two unknown functions of s remain in the contact segment, namely the spatial coordinate σ and the axial force \hat{Q}_1 with corresponding differential equations in the second line of [Eqs. \(14\)](#) and [\(19\)](#), respectively. These two quantities determine all the other values: angle φ , [Eq. \(16\)](#), moment M , [Eq. \(17\)](#), transverse force Q_2 , [Eq. \(18\)](#) and pressure p , [Eq. \(20\)](#). Positions of particles $\mathbf{r}(s)$ follow after substitution of the spatial coordinate $\sigma(s)$ into $\mathbf{R}(\sigma)$, [Eq. \(15\)](#).

3.2. Free segments

Let us turn the attention to the free spans of the right half of the belt, with boundaries $0 \leq s \leq s_1$ for the lower and $s_2 \leq s \leq L/2$ for the upper span. The projected balance of forces retains its general form [Eq. \(11\)](#), but the contact pressure now vanishes, $p = 0$, and we use [Eq. \(12\)](#) to express φ' through M . Because of the symmetry, we know that the transverse shear force Q_2 vanishes in the starting point of the lower free span $s = 0$ and in the end point of the

upper one $s = L/2$. Finally we write the equations for the rotation angle and coordinates (Cartesian components of \mathbf{r}) in the form

$$\begin{aligned}\varphi' &= a^{-1}M, \\ x' &= D \cos \varphi, \\ y' &= D \sin \varphi.\end{aligned}\quad (21)$$

3.3. Formulation of a boundary value problem on a fixed domain

The introduction of a new dimensionless coordinate $0 \leq \xi \leq 1$ allows rewriting the equations in the three segments into one general BVP with fixed boundaries (see Ascher and Russell (1981) for the review of the technique in general, Eliseev and Zinovieva (2012) and Kaczmarczyk and Mirhadizadeh (2016) for applications to static and quasi-static rod contact problems). We transform the above equations by relating the derivatives with respect to s , denoted by a prime, to the derivatives with respect to the new coordinate, written as ∂_ξ , for each segment separately:

$$\begin{aligned}0 \leq s \leq s_1: \quad s &= s_1 \xi \Rightarrow \partial_\xi(\cdots) = s_1(\cdots)', \\ s_1 \leq s \leq s_2: \quad s &= s_1 + \xi(s_2 - s_1) \Rightarrow \partial_\xi(\cdots) = (s_2 - s_1)(\cdots)', \\ s_2 \leq s \leq L/2: \quad s &= L/2 - \xi(L/2 - s_2) \Rightarrow \\ \partial_\xi(\cdots) &= -(L/2 - s_2)(\cdots)';\end{aligned}\quad (22)$$

note that ξ in the upper free segment points in the opposite direction of s , such that both symmetry boundaries $s = 0$ and $s = L/2$ correspond to $\xi = 0$.

We rewrite the equations for all three segments using the above transformation rule and collect them into a single system distinguishing the values by the indices $(\cdots)^{(1)}$, $(\cdots)^{(2)}$, $(\cdots)^{(3)}$ according to the order of segments in Eq. (22). Thus we obtain the BVP for the sixteenth order ODE system:

$$\begin{aligned}\partial_\xi Z &= G(\xi, Z), \\ Z(\xi) &= (\hat{Q}_1^{(1)}, Q_2^{(1)}, M^{(1)}, \varphi^{(1)}, x^{(1)}, y^{(1)}, \sigma^{(2)}, \hat{Q}_1^{(2)}, \\ &\quad \hat{Q}_1^{(3)}, Q_2^{(3)}, M^{(3)}, \varphi^{(3)}, x^{(3)}, y^{(3)}, s_1, s_2)^T.\end{aligned}\quad (23)$$

The variables in the column Z written in Eq. (23) are now considered as functions of ξ again according to Eq. (22). The unknown boundaries $s_{1,2}$ are appended to Z as additional variables with trivial differential equations

$$\partial_\xi s_1 = 0, \quad \partial_\xi s_2 = 0. \quad (24)$$

This step may or may not be necessary depending on the used type of nonlinear BVP solver. Thus, for the finite difference method and BVP solver of Python package Scipy¹ (Kierzenka and Shampine, 2001), the last trivial differential equations are not necessary, and the collocation method with the solver of Matlab package Chebfun (Trefethen et al., 2018) has the support of one unknown constant.

In order to fully state the BVP, we need to provide the boundary conditions for the system Eq. (23). Symmetry considerations at $\xi = 0$ ($s = 0$ for the first segment and $s = L/2$ for the third one) result into

$$\begin{aligned}\xi = 0: \quad \varphi^{(1)} &= 0, \quad x^{(1)} = 0, \quad \varphi^{(3)} = \pi, \\ x^{(3)} &= 0, \quad Q_2^{(1)} = 0, \quad Q_2^{(3)} = 0.\end{aligned}\quad (25)$$

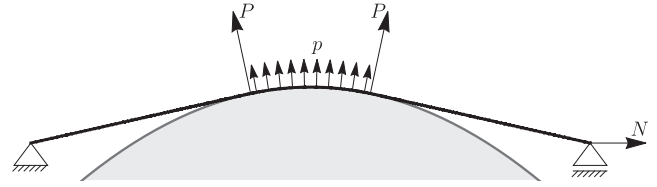


Fig. 2. Bending of a straight beam (thick line) in contact with a rigid cylinder (gray line): the axial tension N results in a continuous zone of contact with distributed contact pressure p and two concentrated contact forces P .

We demand continuity of the geometry, of the bending moment and of the axial force (which also implies continuity of the stretch D) at the boundary s_2 between the second and the third segments:

$$\begin{aligned}\xi = 1: \quad x^{(3)} &= H/2 + R \cos(\sigma^{(2)}/R), \quad y^{(3)} = R \sin(\sigma^{(2)}/R), \\ \varphi^{(3)} &= \pi/2 + \sigma^{(2)}/R, \\ \hat{Q}_1^{(3)} &= \hat{Q}_1^{(2)}, \quad M^{(3)} = aD^{(2)}/R.\end{aligned}\quad (26)$$

At the point with material coordinate s_1 , the dimensionless coordinate ξ in the first segment ($\xi = 1$) differs from the value in the second one ($\xi = 0$). The required continuity leads to the following matching conditions:

$$\begin{aligned}x^{(1)}|_{\xi=1} &= H/2 + R \cos(\sigma^{(2)}/R)|_{\xi=0}, \\ y^{(1)}|_{\xi=1} &= R \sin(\sigma^{(2)}/R)|_{\xi=0}, \\ \varphi^{(1)}|_{\xi=1} &= \pi/2 + \sigma^{(2)}/R|_{\xi=0}, \\ \hat{Q}_1^{(1)}|_{\xi=1} &= \hat{Q}_1^{(2)}|_{\xi=0}, \\ M^{(1)}|_{\xi=1} &= aD^{(2)}/R|_{\xi=0}.\end{aligned}\quad (27)$$

The above boundary conditions allow for jumps in the transverse force Q_2 in the transition points $s_{1,2}$, due to concentrated contact interactions. These jumps indeed appear in the solutions of the BVP, and can be observed in the finite element solutions as well, see discussions of Fig. 7 below.

The full system of Eq. (23) and the boundary conditions (25)–(27) ready for computations are available in the supplementary materials.

Two concentrated contact forces P at the boundaries of the contact zone and a distributed pressure p in between may also be reproduced in the analytical solution of a simple model problem, earlier discussed by Denoël (2008) in a similar setting. Consider small deformation of a simply supported straight beam loaded by a tensile force N and contacting a rigid obstacle in the center, this illustrative example is depicted in Fig. 2. The equilibrium holds owing to the reaction forces in the joints at the end points. Considering $N = 0$ and moving the cylindrical obstacle upwards, we would first observe a single point contact, which may later split into two. The case with tension is easily treated in the framework of a theory for small incremental deflections $w(s)$ from an undeformed, but pre-stressed state, which follows from linearizing the general nonlinear formulation Eqs. (2)–(10). This results in a known equation for the deflection

$$aw''''(s) - Nw''(s) = p(s) \quad (28)$$

see discussion of axially pre-stressed beam-columns with lateral loads in Timoshenko and Gere (1961). Setting the deflection to a prescribed function $w = w_0 - (s - s_0)^2/(2R)$ in the contact zone,

¹ Scipy 1.0.0 documentation. URL: <https://docs.scipy.org/doc/scipy/reference/>. Accessed September 10, 2018

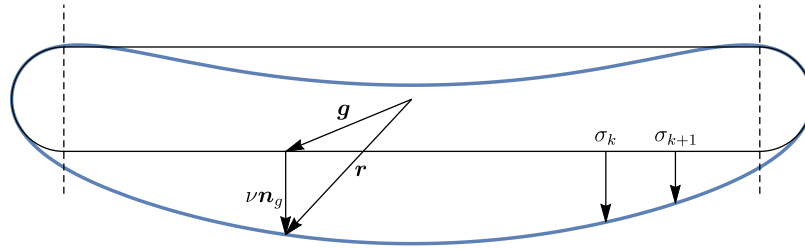


Fig. 4. Finite element discretization: each node has a fixed spatial coordinate σ_k and undergoes a displacement $v\mathbf{n}_g$ from its reference position $\mathbf{g}(\sigma_k)$; dashed lines separate domains with Cartesian and polar coordinates.

to be finer near the contact zones than in the free span regions far away from the pulleys. We discuss the mesh refinement below. Each node k has a fixed coordinate $\sigma_k = \text{const}$. Four nodes are particular in the sense that they reside on the boundaries between the polar and Cartesian domains and move along the dashed lines in Fig. 4. The material particles $s = \text{const}$ may travel across the nodes between neighbouring elements during the deformation according to the variation of \bar{s} .

Each element is bounded by two successive nodes σ_k, σ_{k+1} and belongs to either one of the Cartesian or one of the polar domains, see Fig. 4. Introducing a local coordinate on a finite element ξ , which varies from -1 to 1 , we need to interpolate the geometry of the element by specifying $\sigma(\xi)$. The deformed state is determined by the two unknown fields $\bar{s}(\xi)$ and $v(\xi)$ approximated from the nodal values. The desired smoothness (continuity of \mathbf{r}') implies C^1 continuity of the finite element shape functions. The geometry of a finite element between nodes $k-1$ and k is now approximated according to

$$\sigma = \psi_1(\xi)\sigma_k + \psi_2(\xi)(\partial_\xi \sigma)_k + \psi_3(\xi)\sigma_{k+1} + \psi_4(\xi)(\partial_\xi \sigma)_{k+1}. \quad (34)$$

The nodal slopes $(\partial_\xi \sigma)_k$ define the finite element mesh along with the nodal values σ_k , and the cubic shape functions uniquely follow from the condition

$$\begin{bmatrix} \psi_1(-1) & \partial_\xi \psi_1(-1) & \psi_1(1) & \partial_\xi \psi_1(1) \\ \psi_2(-1) & \partial_\xi \psi_2(-1) & \psi_2(1) & \partial_\xi \psi_2(1) \\ \psi_3(-1) & \partial_\xi \psi_3(-1) & \psi_3(1) & \partial_\xi \psi_3(1) \\ \psi_4(-1) & \partial_\xi \psi_4(-1) & \psi_4(1) & \partial_\xi \psi_4(1) \end{bmatrix} = \begin{bmatrix} 1 & 0 & 0 & 0 \\ 0 & 1 & 0 & 0 \\ 0 & 0 & 1 & 0 \\ 0 & 0 & 0 & 1 \end{bmatrix}; \quad (35)$$

see Vetyukov (2012) and Gruber et al. (2013) for the use of the same approximation in classical in-plane and three-dimensional rod problems.

Now, we compute the material derivative of the position vector Eq. (31), using the rule of differentiation of inverse functions as well as Eqs. (29), (30) and find

$$\begin{aligned} \mathbf{r}' &= \partial_\xi \mathbf{r} \partial_\xi \xi = (\partial_\xi \sigma \partial_\sigma \mathbf{r} + \partial_\xi v \partial_v \mathbf{r})(\partial_\xi s)^{-1} \\ &= (\partial_\xi \sigma (1 + \alpha v) \mathbf{t}_g + \partial_\xi v \mathbf{n}_g)(\partial_\xi s)^{-1}. \end{aligned} \quad (36)$$

Aiming to achieve the desired smoothness of \mathbf{r} , we need to compensate jumps of α in the nodes, which lie on the boundaries between the Cartesian and polar domains. Remembering that α changes from 0 in the Cartesian to R^{-1} in the polar frame, we see that both derivatives $\partial_\xi v$ and $\partial_\xi s$ must jump simultaneously by the factor $1 + R^{-1}v$, which then will cancel out and effectively render \mathbf{r}' continuous. For this sake we introduce a nonlinear approximation for the unknown field variables:

$$\begin{aligned} q &= \psi_1(\xi)q_k + (1 + \alpha v_k)\psi_2(\xi)(\partial_\xi q)_k + \psi_3(\xi)q_{k+1} \\ &\quad + (1 + \alpha v_{k+1})\psi_4(\xi)(\partial_\xi q)_{k+1}. \end{aligned} \quad (37)$$

A variable q , determined by its nodal values, is C^1 continuous inside each particular domain, but its derivative $\partial_\xi q$ jumps exactly

by the factor $1 + R^{-1}v$ in the transition nodes, that separate Cartesian and polar domains. We apply Eq. (37) for $q = v$, and the approximation of the transverse deflections becomes thus quadratic in the polar domains, where $\alpha \neq 0$. The material coordinates s do not directly appear as nodal unknowns, and we use Eq. (37) for the material displacements by setting $q = \bar{s}$. Continuity considerations require an additional solution dependent field $\bar{\sigma}$, which is also approximated according to Eq. (37) from the nodal values σ_k and $(\partial_\xi \sigma)_k$. Comparing to Eq. (34), we see that $\bar{\sigma}$ and σ are identical in the Cartesian domains and coincide in all nodes, as there $\psi_{2,4} = 0$. We use the new variable to update the first relation in Eq. (32), which now reads

$$s = \lambda(\bar{\sigma} + \bar{s}). \quad (38)$$

The entire approximation of the deformed state of the belt is thus nonlinear and determined by the nodal unknowns

$$\bar{s}_k, (\partial_\xi \bar{s})_k, v_k, (\partial_\xi v)_k. \quad (39)$$

To demonstrate, that the above chosen approximation indeed fulfils the continuity requirement for \mathbf{r}' , we now place the first node $k = 1$ in the bottom point of the right pulley $\sigma = 0$ and compute for the left end $\xi = -1$ of the first element in the polar domain (between nodes 1 and 2)

$$\partial_\xi v = (1 + R^{-1}v_1)(\partial_\xi v)_1, \quad \partial_\xi s = \lambda(1 + R^{-1}v_1)((\partial_\xi \sigma)_1 + (\partial_\xi \bar{s})_1). \quad (40)$$

The factor $1 + R^{-1}v_1$ cancels out and Eq. (36) results into

$$\mathbf{r}' = ((\partial_\xi \sigma)_1 \mathbf{t}_g + (\partial_\xi v)_1 \mathbf{n}_g) \lambda^{-1} ((\partial_\xi \sigma)_1 + (\partial_\xi \bar{s})_1)^{-1}. \quad (41)$$

Just the values of the unknowns and of the mesh characteristic $\partial_\xi \sigma$ from the first node remain in the expression. The result will evidently be the same for the right end of the rightmost element of the lower Cartesian region with $\alpha = 0$. This guarantees smoothness of the deformed line of the belt and continuity of the axial strain ε . Expressions for the second order derivatives become slightly cumbersome, which, however, is easy to handle nowadays using computer algebra software and automatic code generation. The curvature is generally discontinuous between the elements for the chosen type of approximation, which does not affect the consistency of the finite element analysis, see discussion in Vetyukov (2012).

6. Finite element solution of the contact problem

Seeking a static equilibrium, we minimize the total strain energy of the belt and its potential energy in the field of gravity such, that the contact conditions are fulfilled. Treating the latter conditions, one chooses between two options. First one is the penalty approach, in which the penetration of the belt into the pulleys is prevented by adding quadratic terms with high coefficients to the aim function of the variational formulation. Second is the approach with Lagrange multipliers, which appear as additional unknown contact forces and may be determined either in the framework

of the classical Newton scheme for the constrained minimization problem or using the method of augmented Lagrangian (Simo and Laursen, 1992), in which the Lagrange multipliers are determined using fixed-point iterations and which is easier to implement. Despite higher complexity, the second approach is traditionally preferred in numerical contact mechanics and we tried implementing it for the problem at hand. Soon it became clear, that the method in its known form does not converge in the presence of concentrated contact interactions, which we also confirmed for the simpler example Fig. 2. The conclusion, that the method of Lagrange multipliers is not suitable for problems involving continuous contact of beams with rigid obstacles, does not appear to be widely known as we were unable to find a reference to it in the published literature on the subject. This finding left us with the simple penalty approach, which appears to be efficient for the problem at hand.

The minimization problem reads

$$U^\Sigma(q) = U^{\text{strain}} + U^{\text{gravity}} + U^{\text{contact}} \rightarrow \min. \quad (42)$$

The aim function depends on the column q of nodal degrees of freedom Eq. (39) and is the sum of the total strain energy

$$U^{\text{strain}} = \int_0^L U \, ds \quad (43)$$

(see Eq. (9) for the definition of the strain energy U per unit material length), of the total potential energy in the field of gravity

$$U^{\text{gravity}} = \int_0^L \rho g y \, ds \quad (44)$$

and of the penalty contact potential

$$U^{\text{contact}} = \int_0^L \frac{1}{2} C \gamma^2 \, ds, \quad \gamma = \max \{R - |\mathbf{r} - H\mathbf{i}/2|, R - |\mathbf{r} + H\mathbf{i}/2|, 0\}. \quad (45)$$

The penetration depth γ is positive in the zones of contact with the pulleys. A high penalty factor C improves the accuracy of fulfilment of the contact condition. Discussing the numerical examples below we will demonstrate, how the numerical solution approaches the exact one with concentrated contact forces when C is increasing, see Fig. 7.

We transform the above integrals first to the spatial description and then to the form, suitable for the finite element scheme:

$$U^{\text{strain}} = \int_0^{L_s} U \partial_\sigma s \, d\sigma = \sum_{f.e.} \int_{-1}^1 U \partial_\xi s (\partial_\xi \sigma)^{-1} \, d\xi, \quad (46)$$

the same transformation applies to Eqs. (44) and (45). The integral over each finite element $-1 \leq \xi \leq 1$ is computed using a Gaussian quadrature rule, 3 integration points were used in the simulation below. The derivative $\partial_\xi s$ is computed using the representation Eq. (38). The derivative of Eq. (34) $\partial_\xi \sigma$ is fixed in each integration point.

We solve the variational problem Eq. (42) using the Newton iterative algorithm, in which new estimates of the equilibrium state q^+ result from a quadratic approximation of the aim function in the vicinity of the previous estimate q^- :

$$\begin{aligned} U^\Sigma &\approx U^\Sigma(q^-) + \left. \frac{\partial U^\Sigma}{\partial q} \right|_{q=q^-} (q - q^-) \\ &+ \frac{1}{2} (q - q^-)^T \left. \frac{\partial^2 U^\Sigma}{\partial q^2} \right|_{q=q^-} (q - q^-) \rightarrow \min, \\ q^+ &= q^- - \left(\left. \frac{\partial^2 U^\Sigma}{\partial q^2} \right|_{q=q^-} \right)^{-1} \left. \frac{\partial U^\Sigma}{\partial q} \right|_{q=q^-}. \end{aligned} \quad (47)$$

The Hesse (stiffness) matrix of second order derivatives becomes ill-conditioned if the penalty factor C is chosen too high, which poses a limit on the accuracy of solution of the contact problem. This matrix may be computed using automatically generated code for expressions of second order derivatives of the strain measures obtained in a computer algebra environment. Nevertheless, the simulations below featured a simpler implementation using numerical differentiation of the first order derivatives, whose algorithmic computation is feasible. This latter approach appears to be sufficiently efficient for the considered static problems with not very high numbers of degrees of freedom.

In the absence of friction the belt may freely move circumferentially, and we had to fix the material point $s = 0$ in the middle node of the lower free span at $x = 0$ by constraining \bar{s} via an additional penalty term in the total energy Eq. (42). The considered example is symmetric, and we actually obtained $s = L/2$ (and $\bar{s} = 0$) in the middle of the upper free span.

7. Benchmark problem and comparison

The parameters of the benchmark example, used for comparison, are (in SI units): $H = 2$, $R = 0.15$, $\lambda = 1.05$, $a = 1/15 = 0.06$, $b = 2000$, $\rho = 0.48$, $g = 9.81$. The actual belt configuration for this set is shown on the left side of Fig. 5 accompanied by solutions for different pre-stretch values λ on the right. Coarse meshes as the one depicted in the figure approximate the displacement field with sufficient accuracy. Nevertheless, derived quantities such as strains or forces call for a finer discretization and it remains yet to explain, how the finite element nodes were arranged along the contour coordinate σ . As pointed out previously, polar and Cartesian regions (separated by a dashed vertical line in the left picture) utilize different finite element approximations. Therefore, we need to foresee nodes at the designated four transition points and consequently mesh each belt segment separately. We apply a constant fine discretization to the polar domains, as the resolution of the contact zones is essential. In the Cartesian regions of the free spans the mesh is gradually coarsened towards the mid points, where nodes are placed in order to enforce the symmetry conditions for the static case. Experimentation with different meshes revealed, that the mesh graduation in the whole model, i.e. the distribution of finite element sizes along the contour coordinate σ , has to be smooth in order that the approximation of strains does not become oscillatory owing to a kind of locking behavior. The configurations obtained for various pre-stretch values as shown on the right side of Fig. 5 illustrate the main quality of the mixed Eulerian-Lagrangian kinematic description, namely: the finite element nodal points only move transversally (blue arrows). They do not take part in the material particle's contour motion, which is exemplarily indicated with red circles for the point initially located at the bottom of the right pulley. Evidently, it floats through the finite element mesh in circumferential direction, while the previously congruent finite element node sticks to its vertical line.

While the above solutions were obtained for the standard, low bending stiffness value a , we study its influence on the hanging configuration of the belt in Fig. 6. It depicts three deformed states

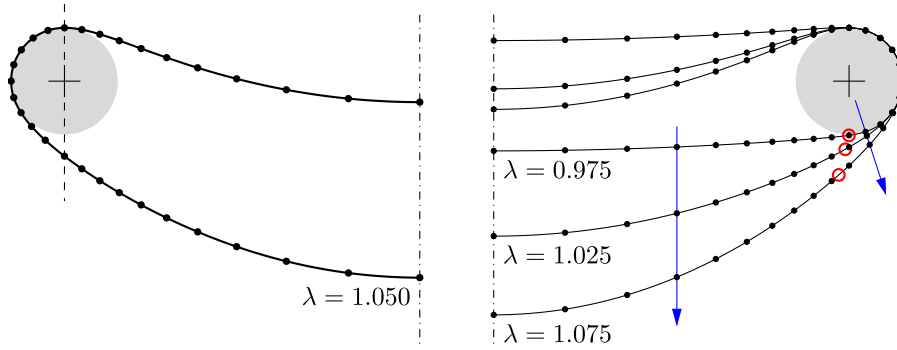


Fig. 5. Deformed configurations of the hanging belt for standard parameters on the left and varying values of the pre-stretch λ on the right; all configurations are symmetric; arrows depict the directions of coordinate lines, along which the nodes may move, and the red circles show the motion of a given material point $s = \text{const}$ as the belt is “inflated” by growing λ . (For interpretation of the references to colour in this figure legend, the reader is referred to the web version of this article.)

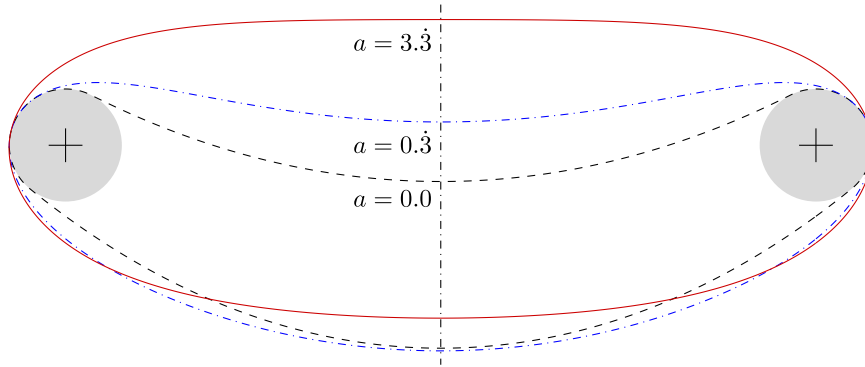


Fig. 6. Deformed configurations of the hanging belt for varying values of the bending stiffness a .

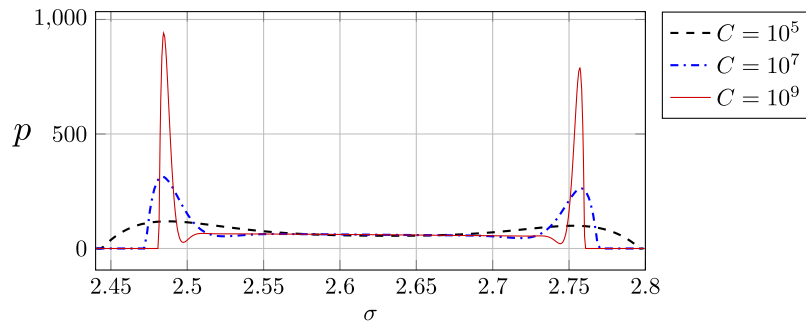


Fig. 7. Contact force distributions for varying penalty factor C .

for different values of the bending stiffness, where $a = 0$ resembles the solution for an ideal string. The bending deformation is dominant at the contact regions, where the belt has to accommodate to the pulleys' geometric curvature. A higher bending stiffness decreases the size of the contact regions, which might even collapse to single points with concentrated contact forces.

Turning to the quantities, which may be derived from the field of displacements, we first study the distribution of the contact forces at the left pulley in Fig. 7; the plot for the opposite side is just mirrored due to symmetry. The contact pressure develops distinct peaks at the touching points, where the first contact of the belt with the pulley occurs. Increasing the penalty stiffness clearly shows, that these needles tend to Dirac-type discontinuities if $C \rightarrow \infty$. This numerically justifies the statement of the semi-analytical treatment, that within unshearable beam theory concentrated contributions to the transverse force occur at the points of first contact with the pulleys, compare Fig. 2. The effect does also prevent us from using the technique of Lagrange multipliers for

the normal contact, as the conventional algorithm with iterative augmentation (Simo and Laursen, 1992) does not converge in this case.

Turning to strains, we plot the distribution of the axial strain measure ε in Fig. 8. The coordinate domains, in which the different finite element approximations reside, are bordered with red vertical lines. The contact region is highlighted with a pale blue colour. The picture contains two graphs for different discretization levels. The solid black line corresponds to a practically converged solution (1032 elements), whereas the faint gray line belongs to a coarser mesh (120 elements, twice as many as in Fig. 5) and reveals disturbing oscillations, that are most pronounced between the right end of the contact segment and the start of the second Cartesian domain. This shall be attributed to the effect of membrane locking of the finite element formulation. The elements struggle to represent the axial strains in regions, where they are most distorted. For example, in the considered case, locking occurs in a domain that is free of contact, yet discretized with elements in polar

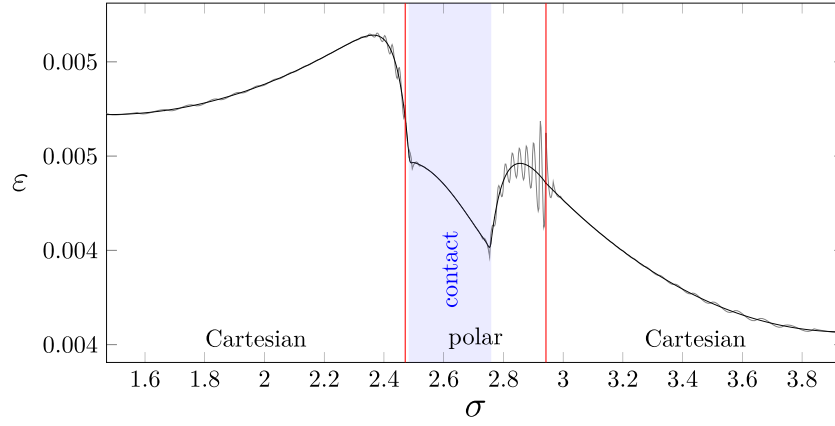


Fig. 8. Distribution of the axial strain measure ε for the left part of the belt drive; phenomenon of membrane locking for coarse meshes (For interpretation of the references to color in this figure, the reader is referred to the web version of this article.).

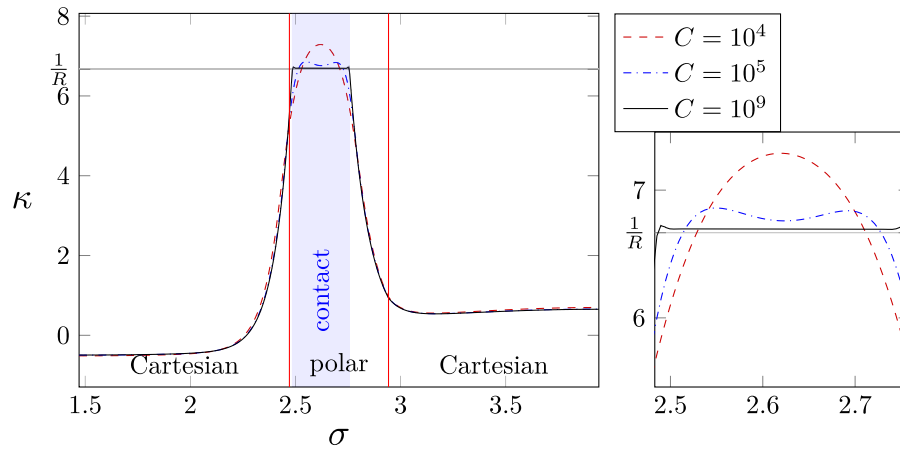


Fig. 9. Distribution of the bending strain measure κ for the left part of the belt drive; impact of the penalty stiffness.

description. These elements “prefer” configurations that are close to a perfect circle, as guaranteed in the contact domain. However, once deformed significantly they can hardly reproduce ε accurately. The same holds true for Cartesian elements, that have to accommodate to a high curvature. However, in the present case the contact region does not extend into the Cartesian coordinate domains and thus the strain irregularities are mainly visible in the polar one.

We have already concluded from Fig. 6, that the bending effects are most accentuated at the pulleys. Consequently the bending strain κ reaches its highest values in the contact domains. We plot its distribution for the left half of the belt in Fig. 9, again indicating different coordinate descriptions as well as the contact domain. The different signs of κ in the free span regions follow from the direction of the outward pointing normal vector \mathbf{n} . The detail picture on the right illustrates the impact of the chosen value of penalty stiffness C . Naturally, small penalty values allow for significant penetration of the belt into the pulley and enforce the belt’s adaption to the pulley’s curvature less strictly. Only minor penetration occurs for the highest value of C and the corresponding black line remains almost constant throughout the contact domain, while keeping a small distance to the geometric curvature $1/R$ due to the axial strain ε .

Lastly, we demonstrate the convergence behaviour of the developed finite elements to the semi-analytically derived results in Fig. 10 by evaluation of the strains at the midpoint of the upper free span $\sigma = 1.47124$. We calculate the error measures

$$\epsilon_\varepsilon = \left| \frac{\varepsilon}{\hat{\varepsilon}} - 1 \right|, \quad \epsilon_\kappa = \left| \frac{\kappa}{\hat{\kappa}} - 1 \right|, \quad (48)$$

with the converged results of the numerical integration of the boundary value problem (see Section 3.4) $\hat{\varepsilon} = 0.00472010$, $\hat{\kappa} = -0.49475014$ and compute the same error measures for reference computations with conventional Lagrangian beam finite elements in global Cartesian coordinates (Vetyukov, 2012). We use constant element sizes for the pure Lagrangian finite element simulations, because locally refined meshes, although applicable in the considered static case, are no longer meaningful when proceeding to simulations with an axially moving belt. By sampling at the middle of the upper free span, the convergence of the mixed Eulerian–Lagrangian finite elements is intentionally tested at a weak point, i.e. the position with greatest element size. Nonetheless, if the nodal points along the contour are distributed properly, the approximations obtained can outreach the results computed with classical finite elements on a constant mesh for a given number of elements. Moreover, the problem-specific mixed kinematic description contributes to the robustness of the applied iterative solver. This effectively enables fast simulations with very coarse meshes, while still retaining a sufficiently high penalty stiffness. The reachable accuracy for the Newton scheme applied to solve the finite element problems at hand is limited by the penalty approach, as high values of the artificial stiffness C promote ill-conditioning. The stagnation of the axial strain error measure on the left of Fig. 10 is thus to be interpreted as a drawback of the penalty method rather

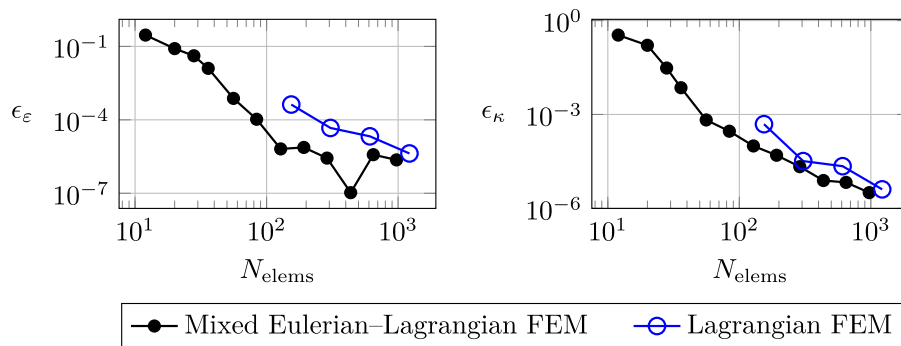


Fig. 10. Convergence study for mixed Eulerian–Lagrangian and conventional Lagrangian beam finite elements in comparison to strain values of the semi-analytically derived results at the middle of the upper free span.

than a deficiency of the mixed finite element description. The slope of both curves in the right picture corresponds to an estimated quadratic order of convergence.

8. Conclusion

We consider a simple planar, symmetric belt drive consisting of a looped, flexible belt hanging on two rigid pulleys. Restricting ourselves to the static problem of the hanging belt in frictionless contact with the pulleys, we employ structural beam theory to deduce a novel semi-analytical solution, which then helps to validate the here developed non-material, mixed Eulerian–Lagrangian finite element scheme.

Making use of the symmetry, we analytically derive a boundary value problem for the remaining half of the belt by application of the beam theory's governing equations to two free span segments and a single contact segment separately. Introduction of a coordinate transformation leads to a standard, nonlinear boundary value problem with known boundaries, which is then solved using several numerical schemes. It turns out, that, as a consequence of the unshearable beam theory, jumps of the transverse force in the points of first contact of the belt with the pulleys appear. This finding can be confirmed considering a simpler problem of geometrically linear beam theory and is also justified by the finite element computations.

In contrast to standard pure Lagrangian finite elements, the mixed finite element formulation utilizes a compound coordinate system consisting of a transversal material coordinate ν and a spatial contour coordinate σ , which runs through Cartesian and polar domains. This coordinate transition across the boundaries with a non-smooth metric of the coordinate system requires nonlinear finite element approximations in order to satisfy the C^1 continuity condition for the displacement field. The nodal points in this mixed finite element mesh do not follow the material points' contour motion, but rather remain at a fixed circumferential coordinate σ and just move transversally with ν . This is beneficial for the future simulations with axially moving belt as it enables the use of inhomogeneous meshes along the axial coordinate and eliminates undesired oscillations of the solution due to material nodal points moving in and out of contact.

The results reveal, that the distribution of element sizes along the contour needs to be smooth. The observed membrane locking at coarse meshes may be a reason for using isogeometric formulations in the future. Validation against the semi-analytical solution demonstrates the robustness of the developed scheme, the quadratic order of convergence and its superiority against pure Lagrangian elements, which will become even more evident when turning to simulations of moving belts with long free spans and small pulleys.

Acknowledgment

This research was partially supported by the Austrian Research Promotion Agency (FFG), project number: 861493. Part of the research done by Evgenii Oborin was carried out in the framework of the joint project of the Russian Foundation for Basic Research (RFBR, Grant No. 14-51-15001) and the Austrian Science Fund (FWF, Grant No. I 2093 International Project).

Supplementary material

Supplementary material associated with this article can be found, in the online version, at doi:10.1016/j.ijsolstr.2019.03.034.

References

- Antman, S., 1972. The Theory of Rods. In: Flügge, S., Truesdell, C. (Eds.), *Handbuch der Physik*, Vol. 2. Springer, Berlin-Heidelberg-New York, pp. 641–703.
- Ascher, U., Russell, R.D., 1981. Reformulation of boundary value problems into “standard” form. *SIAM Rev.* 23 (2), 238–254. doi:10.1137/1023039.
- Batista, M., 2017. Large deflections of an elastic rod in contact with a flat wall. *Int. J. Solids Struct.* 115–116, 53–60.
- Bechtel, S., Vohra, S., Jacob, K., Carlson, C., 2000. The stretching and slipping of belts and fibers on pulleys. *ASME J. Appl. Mech.* 67, 197–206.
- Belyaev, A., Eliseev, V., Irschik, H., Oborin, E., 2017. Contact of two equal rigid pulleys with a belt modelled as cosserat nonlinear elastic rod. *Acta Mech.* 228, 4425–4434.
- Belyaev, A., Eliseev, V., Irschik, H., Oborin, E., 2018. Static contact of belt and pulleys with account for shear and gravity. *J. Phys. Conf. Ser.* 1048 (1), 1–9 <http://stacks.iop.org/1742-6596/1048/i=1/a=012002>.
- Belyaev, A.K., Eliseev, V.V., Irschik, H., Oborin, E., 2017. On static contact of belt and different pulleys. *IOP Conf. Series: Mater. Sci. Eng.* 208 (1), 012004. doi:10.1088/1757-899X/208/1/012004.
- Chen, J.-S., Hua, L.-Y., 2018. Effects of clamping misalignments on the line-contact deformation of a constrained elastica. *Int. J. Nonlinear Mech.* 99, 288–294.
- Chen, L.-Q., 2005. Analysis and control of transverse vibrations of axially moving strings. *ASME Appl. Mech. Rev.* 58, 91–116.
- Denöel, V., 2008. Advantages of a semi-analytical approach for the analysis of an evolving structure with contacts. *Commun. Numer. Methods Eng.* 24 (12), 1667–1683.
- Denöel, V., Detournay, E., 2011. Eulerian formulation of constrained elastica. *Int. J. Solids Struct.* 48, 625–636.
- Dufva, K., Kerkkänen, K., Maqueda, L., Shabana, A., 2007. Nonlinear dynamics of three-dimensional belt drives using the finite-element method. *Nonlinear Dyn.* 48, 449–466.
- Eliseev, V., 2006. *Mechanics of Deformable Solid Bodies* (in russian). St. Petersburg State Polytechnical University Publishing House, St. Petersburg.
- Eliseev, V., Vetyukov, Y., 2012. Effects of deformation in the dynamics of belt drive. *Acta Mech.* 223, 1657–1667. doi:10.1007/s00707-012-0675-3.
- Eliseev, V., Zinovieva, T., 2012. Nonlinear-elastic strain of underwater pipeline in laying process. *Comp. Cont. Mech.* 5 (1), 70–78. doi:10.7242/1999-6691/2012.5.1.9.
- Escalona, J., Orzechowski, G., Mikkola, A., 2018. Flexible multibody modeling of reeving systems including transverse vibrations. *Multibody Syst. Dyn.* 1–27.
- Gasmi, A., Joseph, P.F., Rhyne, T.B., Cron, S.M., 2011. Closed-form solution of a shear deformable, extensional ring in contact between two rigid surfaces. *Int. J. Solids Struct.* 48 (5), 843–853. doi:10.1016/j.ijsolstr.2010.11.018.
- Goss, V., Chaouki, R., 2016. Loading paths for an elastic rod in contact with a flat inclined surface. *Int. J. Solids Struct.* 88–89, 274–282.
- Gruber, P., Nachbagger, K., Vetyukov, Y., Gerstmayr, J., 2013. A novel director-based bernoulli-euler beam finite element in absolute nodal coordinate for-

- mulation free of geometric singularities. *Mech. Sci.* 4, 279–289. doi:10.5194/ms-4-279-2013.
- Hong, D., Ren, G., 2011. A modeling of sliding joint on one-dimensional flexible medium. *Multibody Syst. Dyn.* 26, 91–106.
- Huynen, A., Detournay, E., Denoël, V., 2016. Eulerian formulation of elastic rods. *Proc. R. Soc. A* 472, 1–23.
- Kaczmarczyk, S., Mirhadizadeh, S., 2016. Quasi-stationary mechanics of elastic continua with bending stiffness wrapping on a pulley system. *J. Phys. Conf. Ser.* 721 (1), 012011. doi:10.1088/1742-6596/721/1/012011.
- Kierzenka, J., Shampine, L.F., 2001. A BVP solver based on residual control and the matlab PSE. *ACM Trans. Math. Softw.* 27 (3), 229–316. doi:10.1145/502800.502801.
- Liu, J.-P., Cheng, Z.-B., Ren, G.-X., 2019. Online first, An arbitrary lagrangian Eulerian formulation of a geometrically exact timoshenko beam running through a tube. *Acta Mech.* 1–28.
- Morimoto, T., Iizuka, H., 2012. Rolling contact between a rubber ring and rigid cylinders: mechanics of rubber belts. *Int. J. Mech. Sci.* 54, 234–240.
- Oborin, E., Vetyukov, Y., Steinbrecher, I., 2018. Eulerian description of non-stationary motion of an idealized belt-pulley system with dry friction. *Int. J. Solids Struct.* 147, 40–51.
- Rubin, M., 2000. An exact solution for steady motion of an extensible belt in multipulley belt drive systems. *J. Mech. Des.* 122, 311–316.
- Scheidl, J., Vetyukov, Y., Oborin, E., Krommer, M., Schmidrathner, C., 2018. Mixed Eulerian–Lagrangian description in the statics of a flexible belt with tension and bending hanging on two pulleys. *PAMM* 18 (1).
- Simo, J., Laursen, T., 1992. An augmented lagrangian treatment of contact problems involving friction. *Comput. Struct.* 42 (1), 97–116.
- Steinbrecher, I., Humer, A., Vu-Quoc, L., 2017. On the numerical modeling of sliding beams: a comparison of different approaches. *J. Sound Vib.* 408, 270–290.
- Timoshenko, S., Gere, J., 1961. *Theory of Elastic Stability*, 2nd ed. McGraw-Hill, New-York Ch. 1.
- Trefethen, L.N., Birkisson, Á., Driscoll, T.A., 2018. *Exploring ODEs*. Society for Industrial and Applied Mathematics, Philadelphia.
- Vetyukov, Y., 2012. Hybrid asymptotic-direct approach to the problem of finite vibrations of a curved layered strip. *Acta Mech.* 223 (2), 371–385. doi:10.1007/s00707-011-0562-3.
- Vetyukov, Y., 2018. Non-material finite element modelling of large vibrations of axially moving strings and beams. *J. Sound Vib.* 414, 299–317.
- Vetyukov, Y., Gruber, P., Krommer, M., 2016. Nonlinear model of an axially moving plate in a mixed Eulerian–Lagrangian framework. *Acta Mech.* 227, 2831–2842. doi:10.1007/s00707-016-1651-0.
- Vetyukov, Y., Gruber, P., Krommer, M., Gerstmayr, J., Gafur, I., Winter, G., 2017. Mixed Eulerian–Lagrangian description in materials processing: deformation of a metal sheet in a rolling mill. *Int. J. Numer. Methods Eng.* 109, 1371–1390.
- Vetyukov, Y., Oborin, E., Krommer, M., Eliseev, V., 2017. Transient modelling of flexible belt drive dynamics using the equations of a deformable string with discontinuities. *Math. Comput. Model. Dyn. Syst.* 23 (1), 40–54.